ACCSCIENCE PUBLISHING

International Journal of Bioprinting

RESEARCH ARTICLE

Establishing a framework for the design and fabrication of patient-specific scaffolds targeting partial meniscal defects

Francklin Trindade da Silva[1†], Willian Gonçalves Tsumura[2†], Millena de Cassia Sousa e Silva[3], Anderson Oliveira Lobo[3*], and Thiago Domingues Stocco[2*]

[1]Department of Internal Medicine, Faculty of Medical Sciences, State University of Campinas, Campinas, Brazil

[2]BioRegenera.Lab, Bioengineering Program, Scientific and Technological Institute, Brazil University, São Paulo, SP, Brazil

[3]Interdisciplinary Laboratory for Advanced Materials, Materials Science & Engineering Graduate Program, Federal University of Piauí, Teresina, PI, Brazil

(This article belongs to the *Special Issue: Advances in Bioprinting and Organ-on-a-chip and Applications for Precision Medicine*)

Abstract

Meniscal injuries are a leading cause of knee dysfunction and are commonly treated with partial meniscectomy, which often leads to altered joint biomechanics and early onset osteoarthritis. Current meniscal implants and scaffolds fail to address patient-specific anatomical variations, particularly for partial defects, limiting their clinical effectiveness. This pioneering study introduces the first methodology specifically designed to develop patient-specific scaffolds tailored to partial meniscal injuries, representing a groundbreaking advancement in the field. By using medical imaging and computer-aided design, precise 3D models of injured and intact menisci were created, leveraging the contralateral meniscus as a reference. Scaffolds were fabricated through extrusion-based 3D printing to enable accurate replication of the defect geometry. *Ex vivo* analyses demonstrated the scaffolds' adaptability to diverse defect types and their morphological fidelity to the native tissue. Quantitative assessments revealed minimal deviations, underscoring the precision of the proposed method. This innovative methodology provides a robust framework for developing anatomically precise scaffolds, paving the way for personalized regenerative strategies. Beyond its current application, this method holds potential for creating cell-laden scaffolds, acellular implants, or permanent prosthetic devices, addressing critical challenges in meniscal repair and advancing patient-specific tissue engineering.

Keywords: Bioprinting; Meniscus; Patient-specific modeling; Tissue engineering; Tissue scaffold

†These authors contributed equally to this work.

***Corresponding authors:**
Thiago Domingues Stocco (thiago.stocco@ub.edu.br)

Anderson Oliveira Lobo (lobo@ufpi.edu.br)

Citation: da Silva FT, Tsumura WG, Silva MCS, Lobo AO, Stocco TD. Establishing a framework for the design and fabrication of patient-specific scaffolds targeting partial meniscal defects. *Int J Bioprint*.2025;11(1):556-572. doi: 10.36922/ijb.8109

Received: December 21, 2024
Revised: January 11, 2025
Accepted: January 14, 2025
Published Online: January 15, 2025

Copyright: © 2025 Author(s). This is an Open Access article distributed under the terms of the Creative Commons Attribution License, permitting distribution, and reproduction in any medium, provided the original work is properly cited.

Publisher's Note: AccScience Publishing remains neutral with regard to jurisdictional claims in published maps and institutional affiliations.

1. Introduction

The meniscus plays a pivotal role in knee biomechanics, acting as a critical load distributor, shock absorber, and stabilizer during joint movement. Its biomechanical

properties are intrinsically linked to its unique anatomical geometry, biochemical composition, and extracellular matrix architecture.[1,2] Unfortunately, meniscal injuries are highly prevalent and represent one of the leading causes of knee dysfunction worldwide, often resulting from trauma or degenerative conditions. Due to the meniscus's limited vascularization, particularly in its inner regions, these injuries exhibit a markedly reduced intrinsic healing capacity, presenting a persistent challenge in orthopedic practice.[1,3] Thus, meniscal surgeries rank among the most frequently performed orthopedic procedures globally.[4]

Despite advancements in meniscal repair techniques, such as suturing, these interventions are not universally applicable, often being unfeasible in cases involving poor tissue quality or unfavorable tear locations. As a result, partial meniscectomy remains the standard surgical approach, aiming to alleviate symptoms while preserving as much healthy tissue as possible.[5,6] However, this procedure fundamentally disrupts knee biomechanics, increasing contact pressures on the underlying cartilage and expediting degenerative changes. Thus, while providing short-term symptomatic relief, partial or total meniscectomy is strongly associated with the development of early onset osteoarthritis (OA), one of the most prevalent joint disorders globally, impacting millions of individuals and constituting a leading cause of physical disability worldwide.[7–11] These long-term complications underscore the urgent need for new therapies capable of restoring meniscal function and mitigating the progression of joint degeneration.

Meniscal substitutes and scaffolds have emerged as promising solutions to overcome the inherent limitations of conventional treatments for meniscal injuries. These approaches aim to restore the structural integrity of the meniscus and support joint biomechanics, providing alternatives to mitigate the long-term impact of meniscal loss. While they can offer some degree of articular cartilage protection over varied durations, these interventions are often accompanied by incomplete or compromised regeneration of meniscal tears, alterations in knee biomechanics, and suboptimal restoration of joint function. These strategies have been found to be insufficient to prevent the progression of OA at later stages.[12,13]

The limitations of these approaches vary depending on the type of intervention. For instance, meniscal transplants, often considered for extensive injuries, are hindered by challenges such as the risk of allograft infections, immune rejection, and limited donor availability.[14] Conversely, engineered meniscal scaffolds or implants, while more accessible, frequently exhibit issues such as inadequate mechanical properties and durability, lack of bioactivity, and poor integration with native tissue.[12,13] However, a limitation common to all these strategies is their inability to achieve precise anatomical conformity to the patient's meniscus. For example, current FDA(Food and Drug Administration)-approved meniscal implants, fabricated from natural materials like collagen[15] or synthetic polymers such as polyurethane,[16] are designed with a generic one-size-fits-all approach. These implants often require intraoperative manual shaping to fit the patient's anatomy. This lack of anatomical conformity poses a critical limitation, particularly for partial meniscal defects, where precise size and shape matching are essential for successful outcomes. Thus, generic implants fail to replicate the specific anatomical and morphological characteristics of the native meniscus. This lack of conformity can disrupt joint alignment, increase localized stresses on the articular cartilage, and compromise the meniscus's biomechanical roles of load distribution and stabilization.[2,3,13] Such deviations not only accelerate joint degeneration but also hinder functional recovery, highlighting the critical need for patient-specific solutions tailored to the unique geometry of each meniscus.

Although advancements in patient-specific approaches for meniscal scaffolds have been made, these strategies predominantly focus on total meniscal replacements.[17–19] While full meniscal reconstruction represents an important step forward, it is less aligned with clinical realities, as partial meniscal injuries and subsequent partial meniscectomy are far more prevalent.[20] Despite the potential of these advances, no existing methodology currently addresses the specific needs of partial meniscal defects with patient-specific scaffolds tailored to fit the precise anatomical and morphological characteristics of the lesion site.

Thus, this study aims to introduce the first step-by-step methodology for generating patient-specific scaffolds precisely tailored to partial meniscal defects. By integrating medical imaging, computer-aided design (CAD)-based digital modeling, and 3D printing, the proposed approach establishes a systematic framework that prioritizes anatomical accuracy and clinical relevance. The primary focus of this study is not to assess scaffold performance or material properties but to provide a detailed foundation for developing scaffolds adaptable to various applications, including regenerative strategies that may incorporate cellular components, bioactive materials, or durable structural designs. This methodology, outlined schematically in Figure 1, offers a pathway for advancing personalized solutions in meniscal repair and tissue engineering.

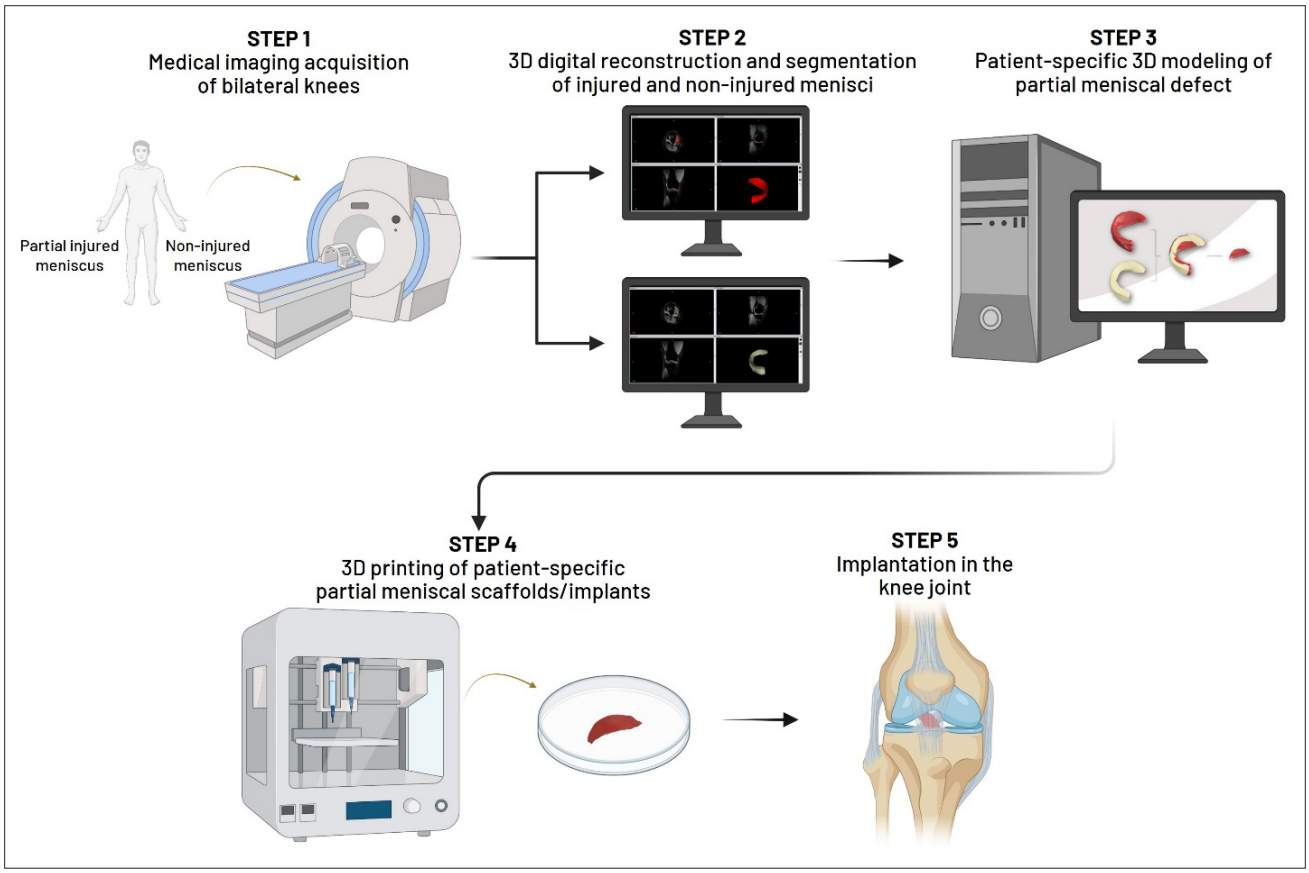

Figure 1. Workflow for developing patient-specific scaffolds/implants for partial meniscal defects. The methodology begins with medical imaging acquisition of bilateral knees to capture both injured and non-injured menisci. The next step involves 3D digital reconstruction and segmentation of the menisci, followed by patient-specific 3D modeling of the partial meniscal defect using the intact contralateral meniscus as a reference. Subsequently, the scaffold/implant is fabricated using 3D printing. The final step is the intended application of the patient-specific scaffold/implant in the knee joint, demonstrating the clinical potential of this approach.

2. Materials and methods

2.1. Digital 3D model generation of partial meniscal defect

The primary objective at this stage is to create a 3D digital model that captures the patient-specific morphology of the medial meniscus, particularly focusing on partial lesions. This process employs magnetic resonance imaging (MRI) images and CAD techniques to translate anatomical data into a customized digital model, accurately reflecting the unique geometry of the meniscal defect. By converting these medical images into a detailed 3D structure, this stage establishes the foundational model required to fabricate a scaffold that closely replicates the native tissue's anatomy and morphology, supporting precision in subsequent biofabrication steps.

2.1.1. Bilateral segmentation and 3D digital reconstruction of menisci

To accurately construct a 3D digital model of the human menisci, a Digital Imaging and Communications in Medicine (DICOM) dataset from a high-resolution bilateral MRI scan of the knee joints (left and right) of an unidentified 30-year-old subject provided by an anonymized database. The MRI included one knee that had undergone partial medial meniscectomy and an intact, uninjured contralateral knee. This dataset was processed using InVesalius (CTI Renato Archer, Brazil) a free, open-source software designed for the visualization, analysis, and 3D reconstruction of medical images from DICOM files. Automatic threshold segmentation was initially applied to identify the meniscal regions, followed by detailed manual adjustments to ensure anatomical precision. The

final 3D reconstructions of the menisci were exported in STL format to facilitate further computational analysis and biofabrication processes.

2.1.2. 3D modeling of partial meniscal scaffold

Following the generation of digital models for both menisci, the next step involved the precise 3D modeling of the partial meniscal defect. This process was performed using Fusion 360 software (Autodesk, USA), which enables detailed manipulation of CAD structures to create an anatomically accurate representation of the lesion site. Initially, both STL files (representing the intact and injured menisci) were aligned centrally within the workspace to ensure consistent orientation. Each STL file was then converted to a solid-body format to enable manipulation required for precise modeling. The healthy meniscus model was subsequently mirrored to match the anatomical side of the injured meniscus. By using Fusion 360's *Combine* function, the overlapping regions between the two models were subtracted, effectively isolating the area of the targeted partial defect. This allowed for the creation of a patient-specific digital scaffold model that accurately represents the missing or damaged portion of the meniscus, providing a foundation for the subsequent stages in the biofabrication process.

2.2. Fabrication of patient-specific partial meniscal scaffold

This step focuses on fabricating a patient-specific scaffold that recaptulates the complex morphology of the meniscal defect previously modeled in three dimensions. Due to the intricate anatomical structure of the meniscus, extrusion-based printing of hydrogel biomaterials was chosen for its ability to achieve controlled deposition and high structural fidelity, essential for reproducing detailed meniscal geometry. This technique is comparatively straightforward and cost-effective, utilizing a pneumatic or mechanical system to dispense the bioink precisely onto the substrate, building sequential layers that form a cohesive three-dimensional structure.[21,22]

2.2.1. Biomaterial ink formulation

Gelatin methacryloyl (GelMA) was selected as the biomaterial matrix for ink formulation due to its favorable properties for bioprinting applications. GelMA, derived from gelatin, a collagen derivative and primary component of the fibrocartilaginous extracellular matrix, is biocompatible, biodegradable, and photocrosslinkable in the presence of a photoinitiator, allowing for extensive customization of its physical and chemical properties.[23,24]

GelMA synthesis was conducted following a previously established protocol, successfully applied, and characterized in our prior studies.[25–27] In brief, type A gelatin from porcine skin (Sigma-Aldrich, USA) was dissolved in phosphate-buffered saline (PBS; Sigma-Aldrich) at 50 °C, with continuous stirring until a homogeneous solution was obtained. Methacrylic anhydride (Sigma-Aldrich, USA) was then added dropwise, and the mixture was stirred for an additional 3 h at 50 °C. The solution was subsequently diluted with preheated PBS, stirred briefly, and then dialyzed against deionized water at 40 °C for 7 days using dialysis tubing (Spectrum Lab Inc., USA) with daily water changes. After dialysis, the solution was lyophilized to yield GelMA as a white solid.

For the final ink formulation, GelMA was dissolved in PBS at a concentration of 100 mg/mL, a concentration shown to support both good printability and cell viability in bioprinting applications.[24,28] To complete the formulation, lithium phenyl-2,4,6-trimethylbenzoylphosphinate (LAP) was added as the photoinitiator at a concentration of 5 mg/mL, ensuring suitability for subsequent bioprinting processes.[29]

2.2.2. Slicing process and adjustment of 3D printing parameters

The next step in the 3D printing process involved slicing the 3D digital model, in which the model was divided into horizontal 2D layers and converted into a G-code file format, a programming language compatible with 3D printers, with precise instructions that guide the bioprinter's movements and material deposition according to user-defined parameters. This slicing was performed using PrusaSlicer 2.8.1 (Prusa Research, Czech Republic), with parameters set as follows: the print head was maintained at 20 °C, the nozzle moved at a speed of 6 mm/s, the layer height was set at 0.2 mm, and an infill density was configured at 40%.

2.2.3. 3D printing of scaffold

The 3D printing process was conducted using the patient-specific digital model of the partial meniscal defect. The GelMA-based biomaterial ink was loaded into 10 mL plastic syringes fitted with conical plastic needles with an inner nozzle diameter of 0.40 mm. An extrusion-based bioprinter (BioEnder Thermo, BioEdTech, Brazil) was employed to fabricate the scaffold structure. During the printing process, the scaffold was exposed to a 405 nm wavelength light source for on-the-spot photocrosslinking to ensure initial structural stability. Following completion of the printing process, the structure was further exposed to the same light source for an additional 2 min to finalize the photocrosslinking of the hydrogel.

2.3. Scanning and quantitative morphological analysis of printed scaffold

To evaluate the printed scaffold's accuracy in replicating the patient-specific meniscal defect, a quantitative morphological comparison was conducted between the nominal 3D digital model and the scanned printed scaffold. The printed meniscal scaffolds were scanned using a structured-light 3D scanner (Dolphin, RVS3D, Brazil), featuring a scanning accuracy of 0.04 mm and a point spacing of 0.06 mm. Each scaffold was scanned in 3 orientations and across 12 rotational positions on a turntable platform to capture a comprehensive representation of the structure. The resulting 3D digital model (in STL format) was then imported into GOM Inspect (GOM GmbH, Germany), a metrology-grade software, to conduct a 3D deviation analysis relative to the nominal model derived from medical imaging data. After fitting and alignment, the morphological similarity of the two models was analyzed using the CAD Comparison tool, with results displayed as a deviation chromatogram, providing a detailed quantitative assessment of morphological fidelity between the printed scaffold and the original digital model.

2.4. Proof-of-concept *ex vivo* implantation analysis

To validate the proposed technique, an *ex vivo* study was conducted, providing essential insights for a successful transition from laboratory development to potential clinical applications (Figure 2).

Initially, bilateral intact porcine knee joints were obtained from a local butcher, and menisci were

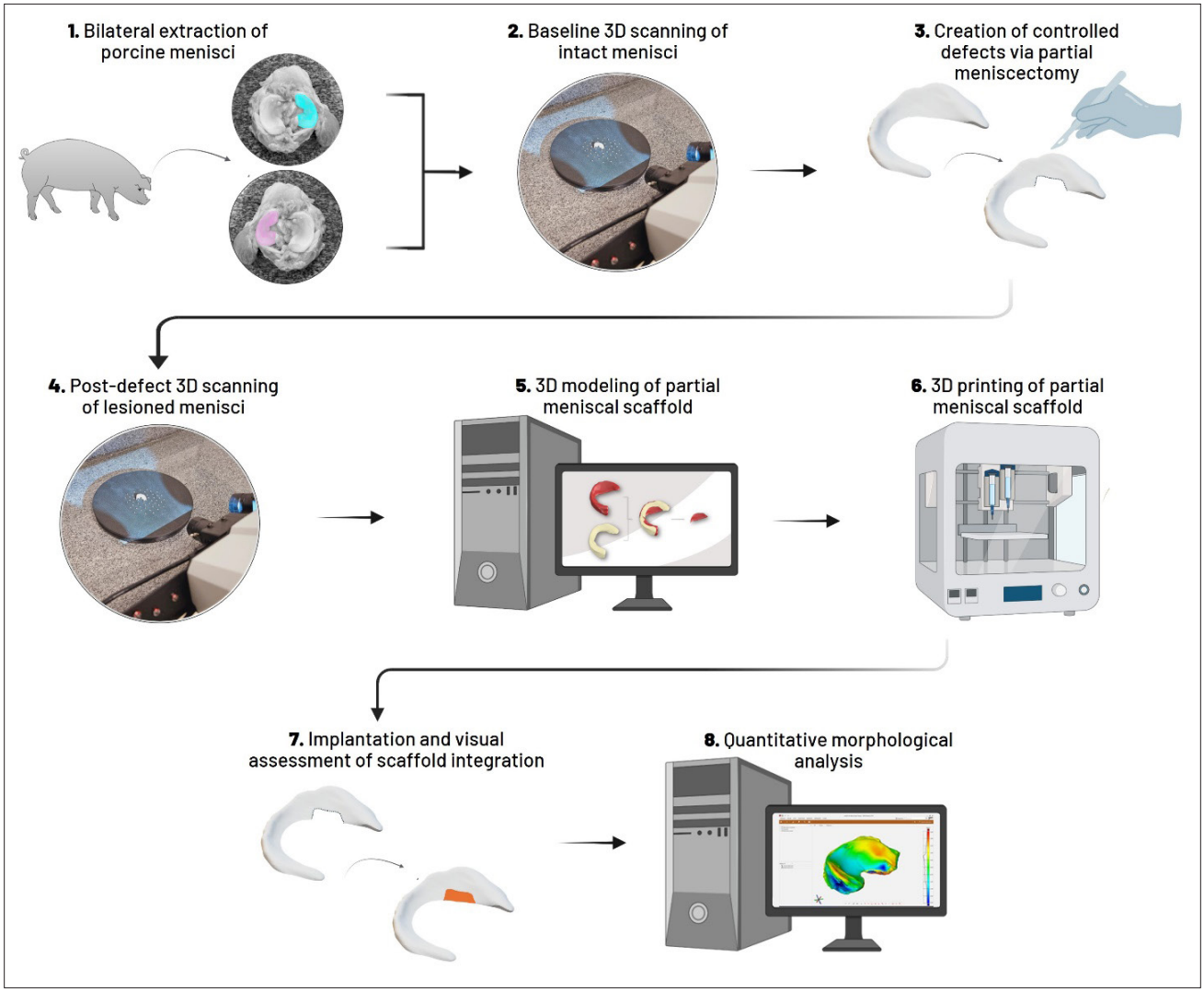

Figure 2. Schematic diagram illustrating the proof-of-concept *ex vivo* study for the initial validation of the proposed methodology for fabricating patient-specific partial meniscal scaffolds.

carefully extracted under sterile conditions to preserve their structural integrity. Each meniscus was scanned using a structured-light 3D scanner as described in **Section 2.3** to establish baseline 3D models of the intact meniscal structures.

Next, a partial meniscectomy was performed on one meniscus from each pair, creating a controlled defect to serve as a receptacle for the patient-specific scaffold implant. The lesioned menisci were then rescanned, and the acquired 3D digital images were processed following the method outlined in **Section 2.1.2**. Then, using the intact contralateral meniscus as a reference, the digital model of the meniscal defect was reconstructed to guide the creation of the scaffold structure tailored to the defect's dimensions and morphology.

Following the modeling stage, 3D printing of the patient-specific scaffold was conducted according to the protocol in **Section 2.2**, resulting in a custom-fit implant designed to restore the meniscus's anatomical continuity. Each scaffold was subsequently implanted into the defect site, and a visual assessment was performed to evaluate the fit and integration of the scaffold across different lesion types, including medial and lateral menisci, as well as varying defect sizes and complexities, such as large, small, and multi-lesion scenarios. This macroscopic analysis provided a qualitative assessment of the scaffold's adaptability to different meniscal geometries and defect profiles, with photographic documentation capturing various fit outcomes.

Finally, quantitative morphological analyses were conducted on the implanted scaffolds to assess their structural fidelity. The scaffold-implanted menisci were scanned post-implantation, and a comparative analysis was performed against the baseline 3D digital model of the intact meniscus using GOM Inspect, as described in **Section 2.3**. This comparison evaluated the precision of scaffold integration by examining deviation patterns between the original, uninjured meniscus and the scaffold-implanted structure, confirming the proposed technique's effectiveness, and identifying areas for potential optimization.

3. Results and discussion

The segmentation and 3D reconstruction of the medial menisci from bilateral MRI scans were successfully performed using InVesalius (CTI Renato Archer) (Figure 3A and B), a free and versatile software tool widely applied in various medical fields. Similar tools for medical segmentation and reconstruction include 3D Slicer, Mimics, and OsiriX[30]; however, InVesalius has been increasingly recognized for its accessibility and functionality, particularly in applications that require precise anatomical modeling, such as craniofacial[31] and brain tissue reconstruction.[32] In previous studies, our research group has effectively employed InVesalius for meniscal segmentation, demonstrating its capability for generating accurate digital models for musculoskeletal applications.[19]

Despite the overall success of the segmentation, we observed limitations in the automatic thresholding feature of InVesalius for this application. While automatic threshold segmentation provided a starting point, significant manual adjustments were necessary to accurately delineate meniscal boundaries, requiring a high level of anatomical expertise to ensure model precision. This need presents a limitation not only for efficiency in larger studies but also for the clinical applicability and translational potential of this methodology. Enhancements to automatic thresholding algorithms, as well as the development of new automated tools, could streamline the segmentation process, reducing the need for extensive manual corrections and improving reproducibility in both research and clinical settings.

In this study, we used high-resolution isotropic MRI images, a sequence type that typically provides slice thicknesses between 0.5 and 1 mm and yields a higher number of slices depending on the anatomical area and settings (our dataset contained 135 slices). This isotropic sequence enables the acquisition of voxels with equal dimensions in all directions, allowing for accurate spatial resolution and high-definition 3D reconstruction.[33] However, conventional MRI protocols for routine knee joint imaging generally employ thicker slices of 3–5 mm, resulting in only 20–40 slices per sequence, and leading to significant anatomical information loss.[34,35] Our preliminary tests using these routine MRI data confirmed that the wider slice spacing introduces continuity issues that hinder accurate 3D modeling. Although high-resolution isotropic MRI addresses these limitations, it is generally impractical for routine use due to time and resource limitations in clinical settings. Future improvements may leverage artificial intelligence (AI) strategies to enhance segmentation accuracy and streamline model reconstruction, including deep learning techniques such as convolutional neural networks (CNNs) and generative adversarial networks (GANs), which have shown promise in super-resolution applications.[36–38] For meniscal imaging specifically, such models could be trained to predict and reconstruct missing spatial information, bridging the gap between clinical imaging limitations and the precision required for patient-specific applications.

The final 3D digital models of the segmented menisci are displayed in Figure 3C and D, accurately representing

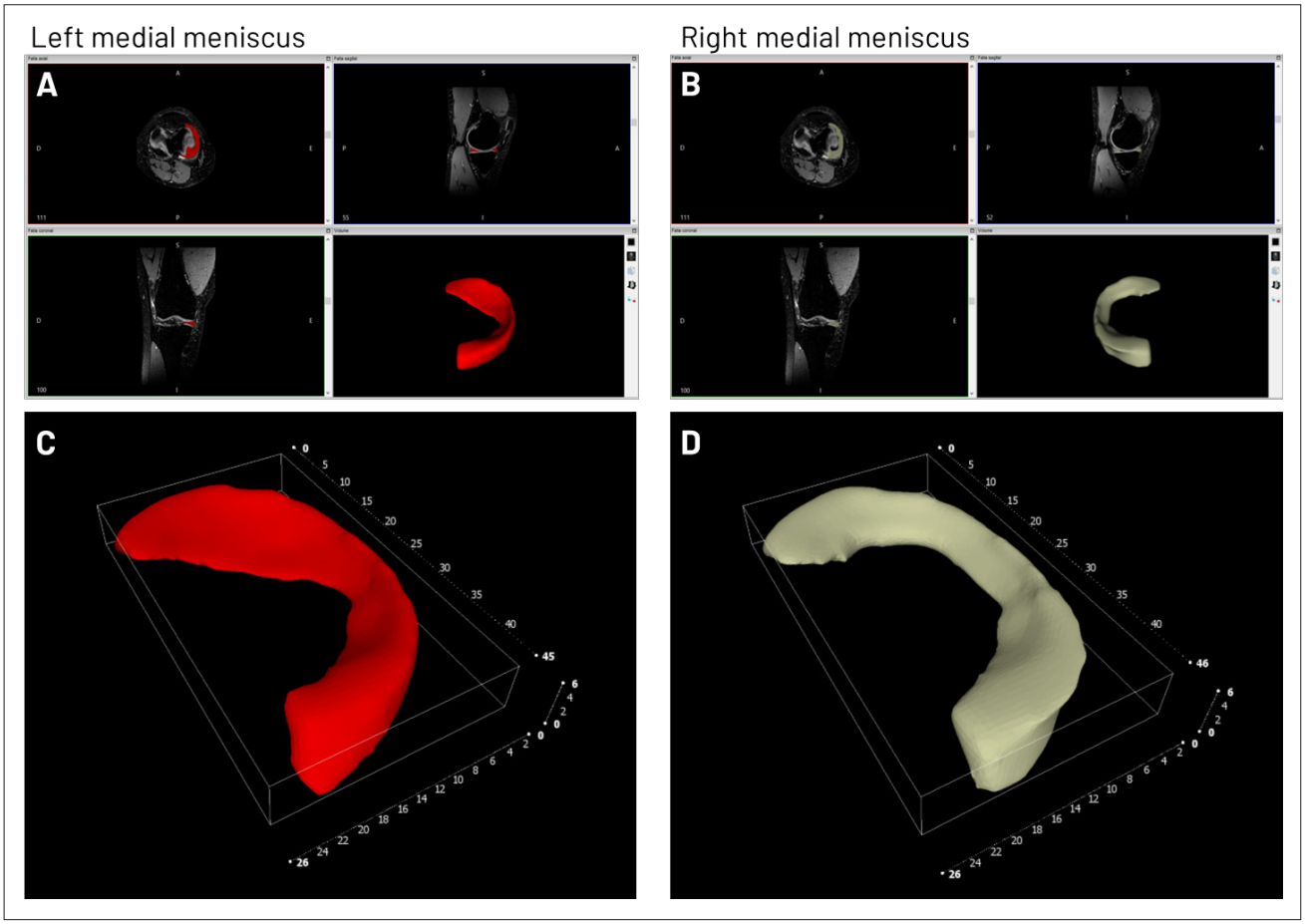

Figure 3. Magnetic resonance imaging (MRI) segmentation and 3D reconstruction of medial menisci from bilateral knee scans. Segmentation and initial 3D reconstruction process of the intact (A) and injured (B) medial menisci. Final 3D digital models of the intact (C) and injured (D) menisci (dimensions displayed in millimeters, mm).

their anatomical structure. Table 1 summarizes the dimensional measurements of the digital meniscus models obtained from each side. Analysis of these dimensions reveals a high degree of morphological similarity between the contralateral menisci, consistent with previous findings in the literature.[39] This previously reported symmetry supports our methodology, using the intact contralateral meniscus as a foundational guide for reconstructing defects in the injured meniscus.

Table 1. Dimensional measurements of 3D reconstructed medial meniscus models for bilateral knee joints

Measurement	Left medial meniscus (intact) (mm)	Right medial meniscus (injured) (mm)
Anterior-posterior length (*x*-axis)	25.65	25.98
Medial-lateral width (*y*-axis)	44.87	45.82
Superior-inferior thickness (*z*-axis)	5.26	5.77

The 3D modeling of the partial meniscal defect was performed to create a patient-specific scaffold that accurately replicates the lesion site, as illustrated in Figure 4A. The digital reconstruction process involved multiple steps to isolate the defective area and generate a custom scaffold model. Figure 4A-I and A-II depict the individual 3D models of the medial menisci: the intact left meniscus (Figure 4A-I) and the partially injured right meniscus (Figure 4A-II). These initial models served as the foundation for aligning, mirroring, and subtracting overlapping regions to generate the final scaffold.

To achieve accurate modeling, both meniscal models were aligned centrally within Fusion 360 software (Autodesk) to ensure consistent orientation, followed by the conversion of STL files to a solid-body format, allowing precise manipulation. In Figure 4A-III, the intact and injured menisci are shown superimposed, providing a

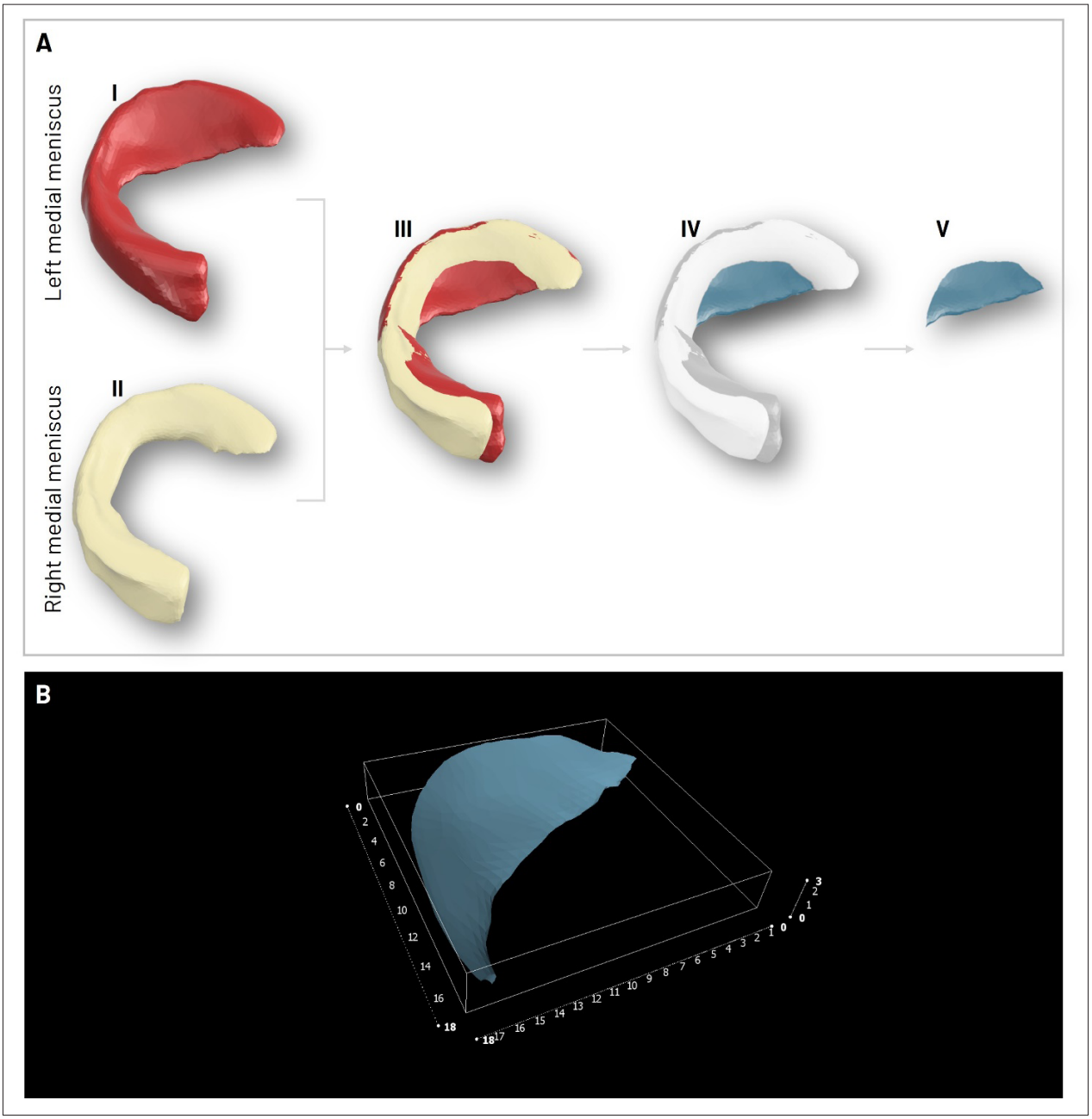

Figure 4. Digital reconstruction and modeling process for a patient-specific meniscal scaffold. (A) Step-by-step modeling of the partial meniscal defect. (I) 3D digital model of the intact left meniscus; (II) 3D model of the partially injured right meniscus; (III) superimposed models of the intact and injured menisci to highlight overlapping regions; (IV) isolation of the partial defect area by subtracting the intact meniscus from the injured one; (V) final extracted defect region used as the foundation for scaffold design. (B) Final patient-specific scaffold model (dimensions displayed in millimeters, mm).

clear view of the overlapping regions. By using the *Combine* function in Fusion 360, we isolated the area of partial meniscectomy by subtracting the intact meniscus from the injured one. This subtraction step is crucial, as it enables the identification of the precise region where tissue loss has occurred, specifically in the inner section of the meniscus, which is highlighted in Figure 4A-IV. Only this region, representing the partial defect, was retained, with other minor discrepancies between the menisci disregarded to maintain anatomical accuracy.

The final output, shown in Figure 4A-V, represents the extracted defect area that will serve as the basis for the scaffold design. The result of the modeling process,

illustrated in Figure 4B, showcases the patient-specific scaffold with precise measurements: a total length of 17.46 mm, a width of 17.19 mm, and a height of 2.69 mm. These dimensions are crucial for ensuring that the scaffold will provide an accurate fit within the lesion site, offering structural support to facilitate meniscal repair.

By using the intact meniscus as a template, we ensured that the scaffold design closely mimics the missing tissue. This approach serves as a potential alternative to other patient-specific modeling strategies, such as freehand digital design or generic templates, which do not use the native tissue as a guide.[40–42] While such methods have their applications, they do not always achieve the anatomical fidelity needed for accurately replicating certain complex structures in the human body, where even small deviations from the original geometry can have a considerable impact on functionality. For meniscal repair, in particular, achieving a high degree of anatomical accuracy is critical, as any discrepancy may impact joint stability and load distribution.[43,44]

Fusion 360 was selected for this study due to its user-friendly interface and interactive tools, facilitating precise alignment and subtraction operations essential for scaffold design. Although a free license for Fusion 360 is currently available for students and educators on a limited basis, the software's commercial nature poses a limitation for broader accessibility. Therefore, to enhance accessibility in future applications, similar modeling routines could be developed using free and open-source software, such as Blender.[45] This adaptation would broaden the applicability of our protocol and make patient-specific scaffold design more attainable in diverse research and clinical settings.

The process of 3D printing the meniscal scaffold is illustrated in Figure 5. Figure 5A shows the 3D model after slicing, ready for extrusion-based printing, while Figure 5B

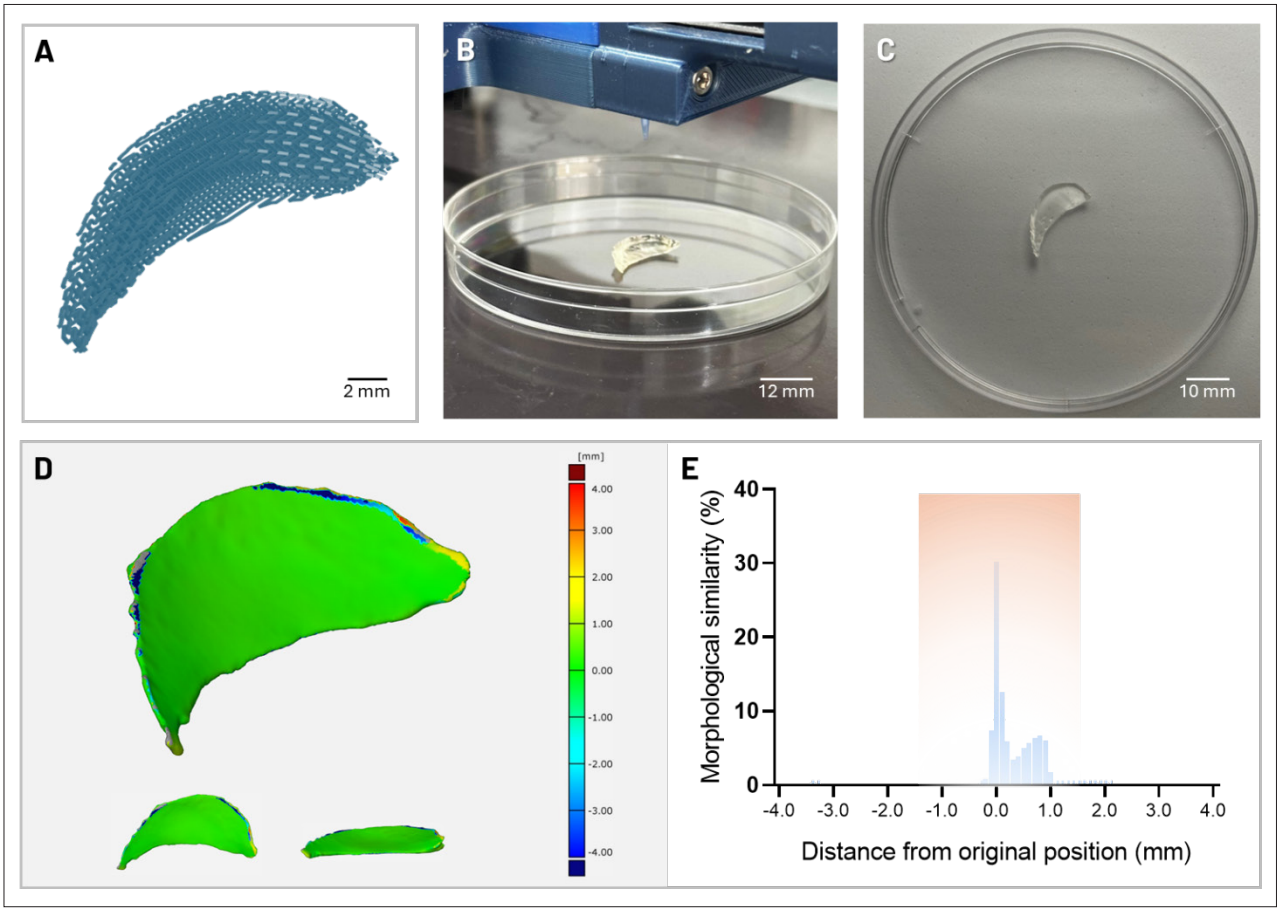

Figure 5. Stages of 3D printing and dimensional accuracy analysis of the meniscal scaffold. (A) Sliced 3D model prepared for extrusion-based printing. (B) Scaffold during the printing process. (C) Final printed scaffold. (D) Color-coded deviation chromatogram generated by GOM Inspect, displaying point-by-point distance deviations between the scanned, printed scaffold, and the nominal digital model (green regions indicate minimal deviation, while blue and red regions highlight areas where the printed scaffold diverges from target dimensions). (E) Histogram quantifying surface deviation (an orange shadow is present in the background of the graph, visually emphasizing and limiting deviations within ±1.5 mm).

captures the scaffold during the printing process, and Figure 5C presents the final printed scaffold. The 3D deviation analysis conducted using GOM Inspect (Figure 5D) provides a color-coded deviation chromatogram, illustrating the point-by-point distance between the 3D model obtained from the scanned, printed scaffold, and the nominal digital model originally designed for printing. This analysis measures the spatial discrepancies at each surface point, enabling us to visualize how closely the printed structure aligns with the intended design. In the chromatogram, green regions indicate minimal deviation, showing that most points on the scaffold's surface align closely with the digital model, while blue and red regions denote negative and positive deviations, respectively, highlighting areas where the printed scaffold deviates from target dimensions. Although this approach provides both quantitative and qualitative insights into scaffold structural accuracy, facilitating high-resolution shape characterization, it remains underexplored for applications in tissue engineering and scaffold validation. This technique is particularly valuable for evaluating scaffold dimensional accuracy and identifying potential areas for refinement, which are crucial for enhancing the precision and reliability of 3D bioprinting in complex tissue constructs. Additionally, its non-destructive nature is especially advantageous for assessing biofabricated tissues, as it allows for precise dimensional verification without compromising the integrity of the scaffold, an essential factor prior to clinical application.

The histogram in Figure 5E quantifies this deviation, showing that 96.84% of the scaffold's surface points deviate by less than ±1.5 mm, underscoring the high fidelity of our 3D printing process. This level of accuracy highlights the effectiveness of our biofabrication process in achieving a structure that closely replicates the digital model. The extrusion-based hydrogel printing method proved effective for fabricating the meniscal partial scaffold. Additionally, this technique permits the incorporation of cells and other components that support the development of functional living tissues and regenerative implants, making it suitable for applications in personalized tissue engineering.[21,22] However, this technique presents challenges, requiring a steep learning curve to achieve consistent results. Factors such as environmental conditions (e.g., temperature and humidity) and variations in the rheological properties of the biomaterial ink add complexity to standardizing the printing process. Currently, we are also actively exploring alternative printing methods, such as digital light processing (DLP), which offers enhanced precision in structural details and could reduce the impact of operator skill and environmental variability on outcomes.[46] Additionally, the extrusion-based approach may encounter significant difficulties when fabricating more complex, patient-specific scaffolds, especially those without a flat base, due to gravitational effects that can distort soft hydrogel structures during printing. Overcoming this limitation may involve exploring other advanced bioprinting strategies, such as freeform reversible embedding of suspended hydrogels (FRESH)[47] and volumetric 3D bioprinting,[48] both of which provide supportive matrices that allow for more intricate scaffold geometries and mitigate gravitational distortion.

Given that evaluating bioink properties was not within the scope of this study, we opted for GelMA hydrogel, a well-established biomaterial for extrusion-based bioprinting. GelMA offers suitable printability and supports cell encapsulation and viability, making it an effective choice for scaffold fabrication in tissue engineering applications.[23] However, GelMA has known limitations regarding mechanical strength, restricting its capacity to mimic the load-bearing properties of native meniscal tissue.[2,49] Both literature data and our previous studies indicate that the mechanical properties of GelMA-based scaffolds could be significantly enhanced through the integration of reinforcing agents, such as nanomaterials, to meet the specific biomechanical demands of meniscal tissue repair.[26,49] Future research could, therefore, focus on optimizing the composition of GelMA or exploring alternative hydrogels to enhance mechanical robustness without compromising biological compatibility within this biofabrication protocol.

The *ex vivo* implantation analysis aimed to validate the proposed technique's clinical potential by testing patient-specific scaffolds within meniscal defects under controlled conditions. Bilateral porcine knee joints were procured, and intact menisci were carefully dissected to preserve structural integrity, serving as reference models for the creation of partial defects. These defects were primarily created in the inner regions of the meniscus (white-white zone), aligning with clinical practice where such areas are most commonly affected and pose greater challenges due to their lack of vascularization and intrinsic healing capacity. Conversely, lesions in the outer regions (red-red zone) were not explored, as their vascular supply allows for better healing potential when repaired through suturing.[6] These defects were varied in terms of location, size, and meniscal region to enable assessment of scaffold adaptability across diverse clinical scenarios. Figure 6 illustrates the visual results of this implantation process across three distinct defect types (column I shows the intact meniscus, column II displays the meniscectomized state, and column III presents the meniscus with the patient-specific scaffold implanted). Figure 6A depicts a large horizontal defect in the inner third of the lateral meniscus; Figure 6B shows a substantial lesion encompassing the anterior horn region

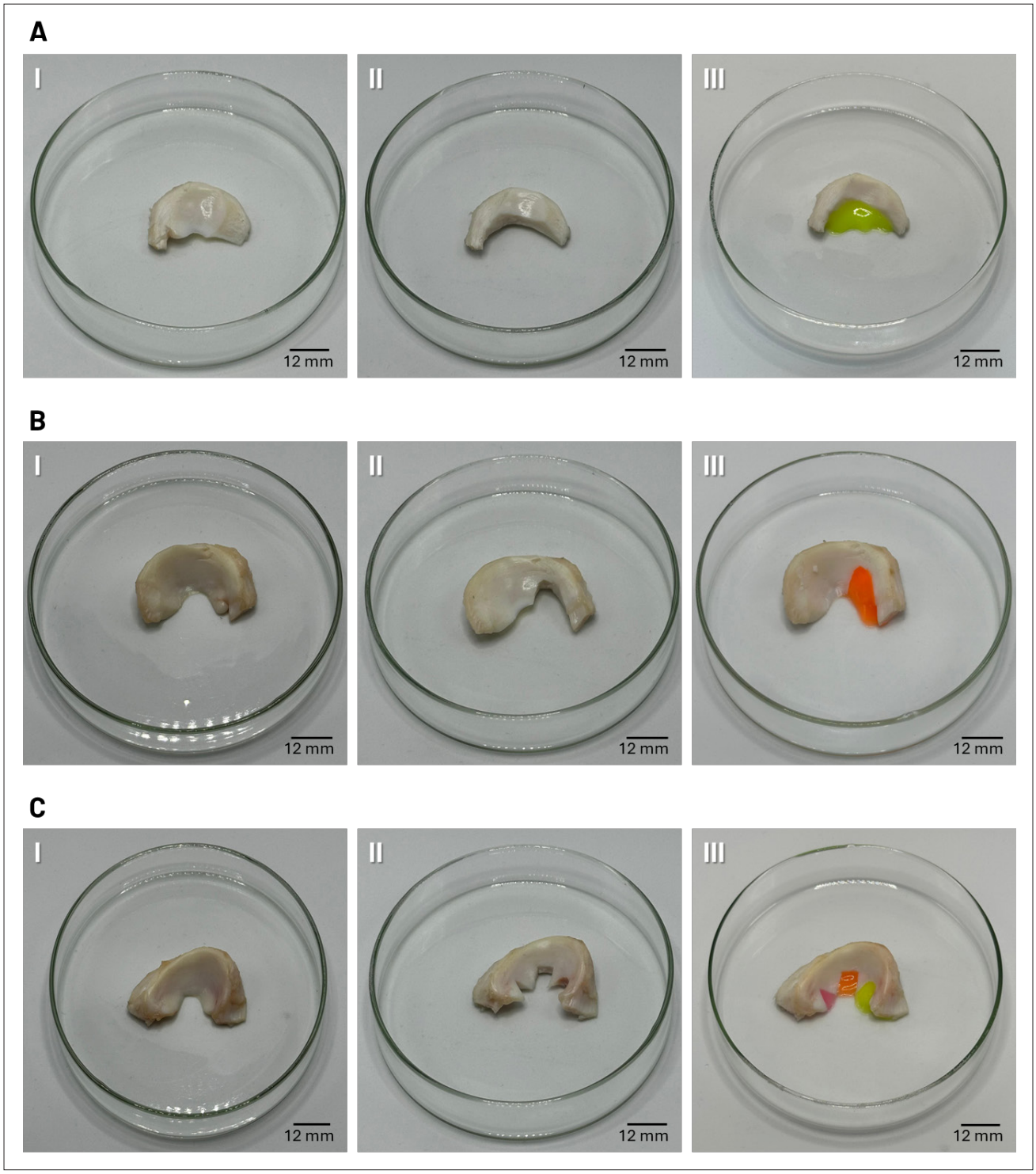

Figure 6. *Ex vivo* implantation of patient-specific scaffolds within partial meniscal defects created in porcine menisci. (A) Large horizontal defect in the inner third of the lateral meniscus. (B) Substantial lesion in the medial third encompassing the anterior horn of the medial meniscus. (C) Multiple smaller lesions in the lateral meniscus, including triangular, rectangular, and circular shapes. Images I show the intact meniscus before lesion creation; Images II display the meniscectomized state; and Images III present the meniscus with the implanted patient-specific scaffold (water-based food dye was applied to scaffolds to enhance visual contrast).

of the medial meniscus; and Figure 6C demonstrates a lateral meniscus with multiple smaller lesions in various shapes (triangular, rectangular, and circular). A water-based food dye was applied to the scaffolds for enhanced visual contrast, facilitating clearer assessment of scaffold integration within each defect.

An additional visual inspection of the scaffold–tissue interface was conducted using optical microscopy to provide a closer look at the contact between the implanted scaffold and the meniscal tissue (Figure 7). The magnified insets in Figure 7 illustrate the boundary for each defect type, suggesting a generally well-aligned interface between the scaffold and native tissue. The visual continuity observed at the scaffold–tissue junction implies that the scaffold conforms reasonably well to the complex contours of each defect, supporting its adaptability in diverse meniscal geometries.

Quantitative morphological assessments of scaffold fidelity are provided in Figure 8. This analysis compared the scaffold-implanted menisci against the baseline 3D model of the intact meniscus. Figure 8A, C, and E displays deviation chromatograms for the scaffold-implanted menisci corresponding to Figure 6A, B, and C, respectively. The color-coded maps illustrate spatial deviations between the scanned, implanted menisci, and the original intact models. Figure 8B, D, and F present histograms quantifying these deviations, offering a clearer understanding of scaffold fidelity. Notably, the deviation analysis across the scaffold surfaces demonstrated high morphological fidelity in each case, with the majority of surface points deviating within ±1.5 mm. Specifically, 94.92% of surface points on the scaffold-implanted lateral meniscus with the large horizontal defect (Figure 8B), 91.48% on the medial meniscus with the extensive anterior horn defect (Figure 8D), and 95.66% on the lateral meniscus with multiple smaller lesions (Figure 8F) remained within this threshold. The morphological analysis in Figure 8 reveals that the scaffold for the anterior horn defect (Figure 8D) exhibited a broader deviation distribution compared to the other cases. This result suggests that anatomical areas with intricate geometries, such as the anterior horn, may pose additional challenges for scaffold accuracy. The increased deviation in this region could be attributed to the scaffold's limited structural support in complex contours, potentially leading to minor misalignment during implantation.

A potential limitation of our methodology for fabricating patient-specific scaffolds is its reliance on the contralateral meniscus as a reference model. This dependency could restrict the approach's applicability in cases where the contralateral meniscus is compromised or unavailable due to bilateral injury or degeneration. Additionally, extrapolating this methodology to other tissues may not always be feasible, particularly for structures or organs that lack a contralateral counterpart. For instance, in organs with a unique anatomical presence within the body, the absence of a mirrored structure limits the ability to generate a patient-specific scaffold based solely on anatomical symmetry. While the current study demonstrates the feasibility of the proposed methodology, further validation with additional datasets, encompassing variations in patient demographics, would enhance its applicability across diverse anatomical features and clinical scenarios. Moreover, further steps are necessary to transition this work toward full *in vivo* validation. This transition will require optimizing the mechanical properties of the scaffold material to withstand physiological loads and integrating biological components to evaluate cellular

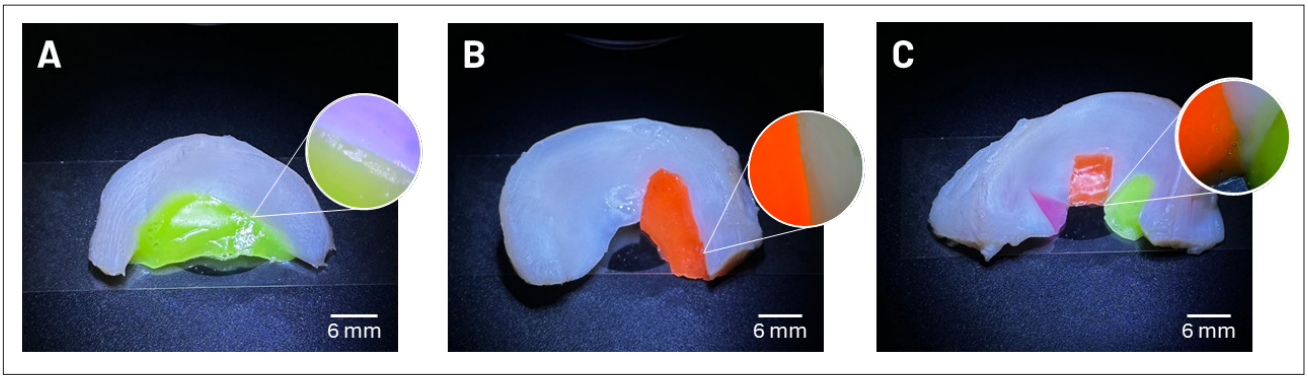

Figure 7. Visual inspection of the scaffold–tissue interface in partial meniscal defects. (A) Large horizontal defect in the inner third of the lateral meniscus. (B) Substantial lesion in the medial third encompassing the anterior horn. (C) Multiple smaller lesions in various shapes within the lateral meniscus. Each image includes a magnified inset captured at 500× magnification using optical microscopy, highlighting the scaffold–tissue interface and demonstrating close contact between the scaffold and meniscal tissue (a water-based dye was applied to the scaffolds to improve visual contrast and facilitate assessment of scaffold integration).

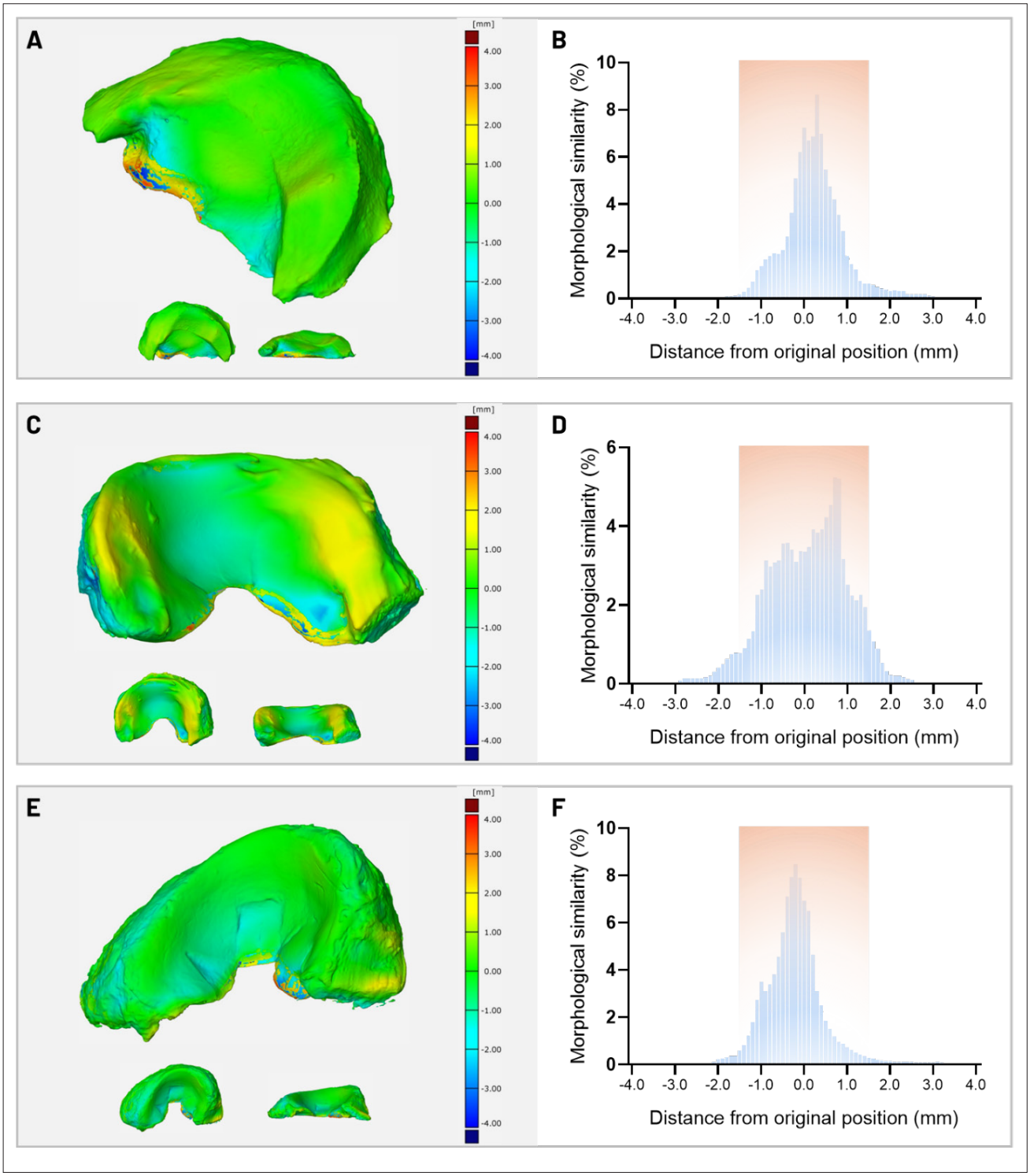

Figure 8. Quantitative morphological analysis of scaffold fidelity using deviation chromatograms and histograms. Deviation chromatograms and corresponding histograms are shown for each scaffold-implanted meniscus: (A, B) lateral meniscus with a large horizontal defect, (C, D) medial meniscus with an extensive defect encompassing the anterior horn, and (E, F) lateral meniscus with multiple smaller lesions. The color-coded maps in the chromatograms illustrate spatial deviations between the scaffold-implanted menisci and their intact 3D models (areas in green represent minor deviation, while blue and red indicate regions where the scaffold deviates more significantly from the intended dimensions), while the histograms quantify the distribution of these deviations (an orange shadow in the background of each histogram highlights and limits deviations within ±1.5 mm).

responses. Expanding these validations will not only strengthen the methodology's clinical applicability but also address critical parameters for its translational potential. Future studies are warranted to address these aspects, building on the foundational work presented here to ensure the methodology's scalability, adaptability, and robustness for broader clinical applications.

Although advances have been made in the field of patient-specific meniscus scaffolds, previous studies have predominantly focused on creating entire meniscal replacements rather than addressing localized, partial defects.[17–19] While some studies have explored scaffolds specifically targeting partial meniscal lesions, these approaches lacked true patient-specific customization in terms of size and morphology.[44,50,51] Therefore, our methodology bridges this gap by combining the patient-specific design of scaffolds with a focus on partial defects. As mentioned above, clinically, partial meniscal injuries are significantly more common, with partial meniscectomy, rather than complete meniscus removal, being the primary surgical intervention.[52] Thus, by developing scaffolds tailored to specific defect sites, our method aligns closely with current clinical practice, aiming to preserve healthy meniscal tissue while minimizing surgical impact. This represents a pioneering step in creating defect-targeted, patient-specific scaffolds for knee menisci with direct clinical relevance.

4. Conclusion

This study successfully presented a novel methodology for creating patient-specific, defect-targeted meniscal scaffolds, addressing a critical gap in regenerative strategies for partial meniscal injuries. By combining medical imaging and CAD-based digital reconstruction, we generated precise 3D models of meniscal defects, enabling the design and fabrication of scaffolds tailored to fit specific lesion sites. The *ex vivo* implantation analysis demonstrated the adaptability of these scaffolds across various defect types and highlighted their morphological fidelity, with quantitative deviation analyses indicating a high degree of structural conformity with the native tissue.

Acknowledgments

The authors gratefully acknowledge BioEdTech company for providing the extrusion-based bioprinter used in this study.

Funding

This work was supported by the National Council for Scientific and Technological Development (CNPq), the Department of Science and Technology of the Ministry of Health (Decit/SECTICS/MS), and the National Program for Genomics and Precision Health (Genomas Brasil) (CNPq: 444141/2023-5). Anderson Oliveira Lobo thanks to CNPq (403890/2023-3 and 310883/2020-2).

Conflict of interest

Thiago Domingues Stocco serves as the Editorial Board Member of the journal and Anderson Oliveira Lobo is the guest editor of the special issue: *Advances in Bioprinting and Organ-on-a-chip and Applications for Precision Medicine*, but did not in any way involve in the editorial and peer-review process conducted for this paper, directly or indirectly. All authors declare that they have no competing interests.

Author contributions

Conceptualization: Thiago Domingues Stocco, Willian Gonçalves Tsumura

Formal analysis: Thiago Domingues Stocco, Francklin Trindade da Silva, Willian Gonçalves Tsumura, Anderson Oliveira Lobo

Funding acquisition: Thiago Domingues Stocco

Investigation: Thiago Domingues Stocco, Francklin Trindade da Silva, Willian Gonçalves Tsumura

Methodology: Thiago Domingues Stocco, Francklin Trindade da Silva, Willian Gonçalves Tsumura, Millena de Cassia Sousa e Silva

Supervision: Thiago Domingues Stocco

Writing–original draft: Thiago Domingues Stocco, Francklin Trindade da Silva, Willian Gonçalves Tsumura, Anderson Oliveira Lobo

Writing–review & editing: Thiago Domingues Stocco, Anderson Oliveira Lobo

Ethics approval and consent to participate

Not applicable.

Consent for publication

Not applicable.

Availability of data

The data that support the findings of this study are openly available on Mendeley Data (http://doi.org/10.17632/zw4b28gpf5.1).

References

1. Fox AJS, Wanivenhaus F, Burge AJ, Warren RF, Rodeo SA. The human meniscus: a review of anatomy, function, injury, and advances in treatment. *Clin Anat*. 2015;28(2):269-287. doi: 10.1002/ca.22456

2. Schwer J, Ignatius A, Seitz AM. The biomechanical properties of human menisci: a systematic review. *Acta Biomater*. 2024;175:1-26.
doi: 10.1016/j.actbio.2023.12.010

3. Pasiński M, Zabrzyńska M, Adamczyk M, et al. A current insight into human knee menisci. *Transl Res Anat*. 2023;32:100259.
doi: 10.1016/j.tria.2023.100259

4. Adams BG, Houston MN, Cameron KL. The epidemiology of meniscus injury. *Sports Med Arthrosc*. 2021;29(3): e24-e33.
doi: 10.1097/JSA.0000000000000329

5. Bergstein VE, Ahiarakwe U, Haft M, Mikula JD, Best MJ. Decreasing Incidence of Partial Meniscectomy and Increasing Incidence of Meniscus Preservation Surgery From 2010 to 2020 in the United States. *Arthroscopy*. 2024: S0749-8063(24)00558-9.
doi: 10.1016/j.arthro.2024.07.030

6. Ozeki N, Seil R, Krych AJ, Koga H. Surgical treatment of complex meniscus tear and disease: state of the art. *J ISAKOS*. 2021;6(1):35-45.
doi: 10.1136/jisakos-2019-000380

7. Ha AY, Shalvoy RM, Voisinet A, Racine J, Aaron RK. Controversial role of arthroscopic meniscectomy of the knee: a review. *World J Orthop*. 2016;7(5):287.
doi: 10.5312/wjo.v7.i5.287

8. Roemer FW, Kwoh CK, Hannon MJ, et al. Partial meniscectomy is associated with increased risk of incident radiographic osteoarthritis and worsening cartilage damage in the following year. *Eur Radiol*. 2017;27(1):404-413.
doi: 10.1007/s00330-016-4361-z

9. Abram SGF, Judge A, Beard DJ, Price AJ. Adverse outcomes after arthroscopic partial meniscectomy: a study of 700 000 procedures in the national Hospital Episode Statistics database for England. *Lancet*. 2018;392(10160):2194-2202.
doi: 10.1016/S0140-6736(18)31771-9

10. Courties A, Kouki I, Soliman N, Mathieu S, Sellam J. Osteoarthritis year in review 2024: epidemiology and therapy. *Osteoarthr Cartil*. 2024;32(11):1397-1404.
doi: 10.1016/j.joca.2024.07.014

11. Hunter DJ, Schofield D, Callander E. The individual and socioeconomic impact of osteoarthritis. *Nat Rev Rheumatol*. 2014;10(7):437-441.
doi: 10.1038/nrrheum.2014.44

12. Bian Y, Cai X, Zhou R, et al. Advances in meniscus tissue engineering: towards bridging the gaps from bench to bedside. *Biomaterials*. 2025;312:122716.
doi: 10.1016/j.biomaterials.2024.122716

13. van Minnen BS, van Tienen TG. The current state of meniscus replacements. *Curr Rev Musculoskelet Med*. 2024;17(8):293-302.
doi: 10.1007/s12178-024-09902-1

14. Kani KK, Porrino JA, Chew FS. Meniscal allograft transplantation: a pictorial review. *Curr Probl Diagn Radiol*. 2022;51(5):779-786.
doi: 10.1067/j.cpradiol.2021.09.008

15. Lucidi GA, Grassi A, Agostinone P, et al. Risk factors affecting the survival rate of collagen meniscal implant for partial meniscal deficiency: an analysis of 156 consecutive cases at a mean 10 years of follow-up. *Am J Sports Med*. 2022;50(11):2900-2908.
doi: 10.1177/03635465221112635

16. Accadbled F, Pham TT, Thevenin Lemoine C, Sales de Gauzy J. Implantation of an Actifit® polyurethane meniscal scaffold 18 months after subtotal lateral meniscectomy in a 13-year-old male adolescent. *Am J Case Rep*. 2020; 21:e920688.
doi: 10.12659/AJCR.920688

17. Cengiz IF, Pitikakis M, Cesario L, et al. Building the basis for patient-specific meniscal scaffolds: from human knee MRI to fabrication of 3D printed scaffolds. *Bioprinting*. 2016;1-2:1-10.
doi: 10.1016/j.bprint.2016.05.001

18. Filardo G, Petretta M, Cavallo C, et al. Patient-specific meniscus prototype based on 3D bioprinting of human cell-laden scaffold. *Bone Joint Res*. 2019;8(2):101-106.
doi: 10.1302/2046-3758.82.BJR-2018-0134.R1

19. Stocco TD, Moreira Silva MC, Corat MAF, Gonçalves Lima G, Lobo AO. Towards bioinspired meniscus-regenerative scaffolds: engineering a novel 3D bioprinted patient-specific construct reinforced by biomimetically aligned nanofibers. *Int J Nanomedicine*. 2022;17:1111-1124.
doi: 10.2147/IJN.S353937

20. Jha V. Editorial commentary: rate of meniscal repair versus meniscectomy has improved and should continue to improve. *Arthrosc J Arthrosc Relat Surg*. Published online October 2024: S0749-8063(24)00787-4.
doi: 10.1016/j.arthro.2024.10.006

21. Zhang YS, Haghiashtiani G, Hübscher T, et al. 3D extrusion bioprinting. *Nat Rev Methods Prim*. 2021;1(1):75.
doi: 10.1038/s43586-021-00073-8

22. Huang G, Zhao Y, Chen D, et al. Applications, advancements, and challenges of 3D bioprinting in organ transplantation. *Biomater Sci*. 2024;12(6):1425-1448.
doi: 10.1039/D3BM01934A

23. Das S, Valoor R, Jegadeesan JT, Basu B. 3D bioprinted GelMA scaffolds for clinical applications: promise and challenges. *Bioprinting*. 2024;44:e00365.
doi: 10.1016/j.bprint.2024.e00365

24. Dobrisan MR, Lungu A, Ionita M. A review of the current state of the art in gelatin methacryloyl-based printing inks in bone tissue engineering. *Virtual Phys Prototyp*. 2024;19(1):e2378003.
doi: 10.1080/17452759.2024.2378003

25. Afewerki S, Bassous N, Harb SV, et al. Engineering multifunctional bactericidal nanofibers for abdominal hernia repair. *Commun Biol*. 2021;4(1):233. doi: 10.1038/s42003-021-01758-2

26. e Silva M de CS, de Sousa GF, das Virgens Santana M, Tsumura WG, Stocco TD, Lobo AO. Tailoring mechanical properties of printed GelMA scaffolds with multilayers of PLA/Laponite nanocomposite fibers. *Mater Lett*. 2024;364:136314. doi: 10.1016/j.matlet.2024.136314

27. Montesdeoca CYC, Afewerki S, Stocco TD, et al. Oxygen-generating smart hydrogels supporting chondrocytes survival in oxygen-free environments. *Colloids Surfaces B Biointerfaces*. 2020;194:111192. doi: 10.1016/j.colsurfb.2020.111192

28. Rajabi N, Rezaei A, Kharaziha M, et al. Recent advances on bioprinted gelatin methacrylate-based hydrogels for tissue repair. *Tissue Eng Part A*. 2021;27(11-12):679-702. doi: 10.1089/ten.tea.2020.0350

29. Elkhoury K, Zuazola J, Vijayavenkataraman S. Bioprinting the future using light: a review on photocrosslinking reactions, photoreactive groups, and photoinitiators. *SLAS Technol*. 2023;28(3):142-151. doi: 10.1016/j.slast.2023.02.003

30. Buffinton CM, Baish JW, Ebenstein DM. An introductory module in medical image segmentation for BME students. *Biomed Eng Educ*. 2023;3(1):95-109. doi: 10.1007/s43683-022-00085-0

31. Yap Abdullah J, Manaf Abdullah A, Zaim S, et al. Three-dimensional analysis of reconstructed skulls using three different open-source software versus commercial software. *Proc Inst Mech Eng Part H J Eng Med*. 2024;238(1):55-62. doi: 10.1177/09544119231212034

32. Gür Y. Masked stereolithography 3D printing of a brain tissue from an MRI data set. *Alexandria Eng J*. 2024;98:302-311. doi: 10.1016/j.aej.2024.05.002

33. Bajaj S, Chhabra A, Taneja AK. 3D isotropic MRI of ankle: review of literature with comparison to 2D MRI. *Skeletal Radiol*. 2024;53(5):825-846. doi: 10.1007/s00256-023-04513-2

34. Ai T, Zhang W, Priddy NK, Li X. Diagnostic performance of CUBE MRI sequences of the knee compared with conventional MRI. *Clin Radiol*. 2012;67(12):e58-e63. doi: 10.1016/j.crad.2012.07.020

35. Parkar AP, Adriaensen MEAPM. ESR essentials: MRI of the knee—practice recommendations by ESSR. *Eur Radiol*. 2024;34(10):6590-6599. doi: 10.1007/s00330-024-10706-7

36. Heckel R, Jacob M, Chaudhari A, Perlman O, Shimron E. Deep learning for accelerated and robust MRI reconstruction. *Magn Reson Mater Physics, Biol Med*. 2024;37(3):335-368. doi: 10.1007/s10334-024-01173-8

37. Zhang H, Shinomiya Y, Yoshida S. 3D MRI reconstruction based on 2D generative adversarial network super-resolution. *Sensors*. 2021;21(9):2978. doi: 10.3390/s21092978

38. Küstner T, Qin C, Sun C, Ning L, Scannell CM. The intelligent imaging revolution: artificial intelligence in MRI and MRS acquisition and reconstruction. *Magn Reson Mater Physics, Biol Med*. 2024;37(3):329-333. doi: 10.1007/s10334-024-01179-2

39. Yoon JR, Jeong HI, Seo MJ, et al. The use of contralateral knee magnetic resonance imaging to predict meniscal size during meniscal allograft transplantation. *Arthroscopy*. 2014;30(10):1287-1293. doi: 10.1016/j.arthro.2014.05.009

40. Nimeskern L, Feldmann EM, Kuo W, et al. Magnetic resonance imaging of the ear for patient-specific reconstructive surgery. In: Najbauer J, ed. *PLoS One*. 2014;9(8):e104975. doi: 10.1371/journal.pone.0104975

41. Laubach M, Suresh S, Herath B, et al. Clinical translation of a patient-specific scaffold-guided bone regeneration concept in four cases with large long bone defects. *J Orthop Transl*. 2022;34:73-84. doi: 10.1016/j.jot.2022.04.004

42. Holz J, Spalding T, Boutefnouchet T, et al. Patient-specific metal implants for focal chondral and osteochondral lesions in the knee; excellent clinical results at 2 years. *Knee Surgery, Sport Traumatol Arthrosc*. 2021;29(9):2899-2910. doi: 10.1007/s00167-020-06289-7

43. Mameri ES, Dasari SP, Fortier LM, et al. Review of meniscus anatomy and biomechanics. *Curr Rev Musculoskelet Med*. 2022;15(5):323-335. doi: 10.1007/s12178-022-09768-1

44. Veronesi F, Di Matteo B, Vitale ND, et al. Biosynthetic scaffolds for partial meniscal loss: a systematic review from animal models to clinical practice. *Bioact Mater*. 2021;6(11):3782-3800. doi: 10.1016/j.bioactmat.2021.03.033

45. Martínez Cendrero A, Franco Martínez F, Solórzano Requejo WG, Díaz Lantada A. Open-source library of tissue engineering scaffolds. *Mater Des*. 2022;223:111154. doi: 10.1016/j.matdes.2022.111154

46. Li W, Wang M, Ma H, Chapa-Villarreal FA, Lobo AO, Zhang YS. Stereolithography apparatus and digital light processing-based 3D bioprinting for tissue fabrication. *iScience*. 2023;26(2):106039. doi: 10.1016/j.isci.2023.106039

47. Shiwarski DJ, Hudson AR, Tashman JW, Feinberg AW. Emergence of FRESH 3D printing as a platform for advanced tissue biofabrication. *APL Bioeng*. 2021;5(1):010904. doi: 10.1063/5.0032777

48. Bernal PN, Delrot P, Loterie D, et al. Volumetric bioprinting of complex living-tissue constructs within seconds. *Adv Mater*. 2019;31(42):e1904209.
doi: 10.1002/adma.201904209

49. Guo A, Zhang S, Yang R, Sui C. Enhancing the mechanical strength of 3D printed GelMA for soft tissue engineering applications. *Mater Today Bio*. 2024;24:100939.
doi: 10.1016/j.mtbio.2023.100939

50. Bandyopadhyay A, Mandal BB. A three-dimensional printed silk-based biomimetic tri-layered meniscus for potential patient-specific implantation. *Biofabrication*. 2019;12(1):015003.
doi: 10.1088/1758-5090/ab40fa

51. Bandyopadhyay A, Ghibhela B, Shome S, Pal D, Nandi SK, Mandal BB. Silk-based injectable photocurable hydrogel loaded with autologous growth factors for patient-specific repair of meniscal defects in vivo. *Appl Mater Today*. 2024;37:102111.
doi: 10.1016/j.apmt.2024.102111

52. Avila A, Vasavada K, Shankar DS, Petrera M, Jazrawi LM, Strauss EJ. Current controversies in arthroscopic partial meniscectomy. *Curr Rev Musculoskelet Med*. 2022;15(5):336-343.
doi: 10.1007/s12178-022-09770-7